Journal of Structural Geology, Vol. 2, No. 4, 1980, pp. 425 to 438
Pergamon Press Ltd. 1980. Printed in Great Britain

0191-8141/80/1201-0425 $02.00/0

Numerical models of hydraulic fracturing and the interpretation of syntectonic veins

ALASTAIR BEACH

Department of Geology, The University, P.O. Box 147, Liverpool L69 3BX, England

(*Received* 3 *July* 1979; *accepted in revised form* 11 *June* 1980)

Abstract—The hydraulic fracture is modelled as an ellipse in an infinite elastic medium with an internal fluid pressure and loaded under biaxial stresses at infinity. The available stress function for this model has been evaluated numerically, and the magnitudes of the stresses generated around the crack calculated for a variety of loading conditions and crack orientations. Fracture initiation is predicted from the Griffith maximum tensile stress criterion. The location of the maximum tensile stress around the crack is recorded and it is found that for many conditions of applied stresses and crack fluid pressure, the hydraulic shear fracture has a symmetrically developed maximum tensile stress and fracture initiation will occur by growth along the direction of the crack. It is also predicted that fracture initiation will occur when the ratio of fluid pressure to applied least principal stress is considerably less than one. The elastic strain energy fields around elliptical hydraulic flaws have been calculated, and in particular, the change in strain energy upon introduction of a small flaw, and the change in strain energy upon growth of this flaw, have been investigated. The results allow an evaluation of the second part of the Griffith criterion—that fracture growth is accompanied by a decrease in strain energy—for hydraulic fractures. Changes in strain energy with small increases in fluid pressure provide a physical basis for dilatancy hardening and fracture instability. Quasi-static growth from a flaw is modelled by calculating changes in strain energy for unit increases in half length. The distinction between fractures which show an increasing and a decreasing rate of change in strain energy with increasing length, and between fractures which may only extend spontaneously for short distances and those which may show extensive spontaneous growth on the basis of the rate of change of strain energy with length, is made. A gradual drop in crack fluid pressure once the threshold for fracture initiation has been passed may promote the extent to which spontaneous crack growth occurs.

The formation of syntectonic veins, particularly in rocks being deformed under low grade metamorphic conditions, is often the most abundant evidence of natural hydraulic fracturing in rocks. Commonly observed geometric features of syntectonic veins—length, simple tapering, symmetric and asymmetric forking, branching, irregular zig-zag traces, en échelon patterns—are discussed primarily with reference to the strain energy model for growth established, and the geometric variation is interpreted in terms of variation in applied stress and fluid pressure conditions and the rate of change of stored strain energy with crack growth. In particular, terminal branching arises when the minimum stress changes from a symmetric to an asymmetric location at the tip of a growing shear fracture, and terminal forking results when there is an increase in the energy release rate during crack growth, and may be symmetric or asymmetric depending on the location of the minimum stress at the crack tip at the time of forking.

INTRODUCTION

HYDRAULIC fracturing describes the process of fracturing in which load parallel (tensile) or load oblique (shear) fractures are produced through the action of a fluid under pressure within the crack. Hydraulic fracturing of rocks occurs during the burial, dewatering and metamorphism of sedimentary sequences as very large volumes of fluid are released (Holland & Lambert 1969, Price 1975, Magara 1975a, 1976, Fyfe 1976, Norris & Henley 1976), and also during the formation of many magmatic sheet intrusions (Pollard 1973a, 1979, Escher *et al.* 1976). Hydraulic fracturing has also been developed as an engineering technique to increase productivity in oil and gas fields (Howard & Fast 1970). In general, an increase in the pressure of the fluid within a crack in a material under triaxial compression will reduce the stresses acting on the fracture through the law of effective stress until the crack becomes unstable and propagates. This approach to the mechanics of hydraulic fracturing is dealt with by Hubbert & Willis (1975), Haimson & Fairhurst (1967), Secor (1968), Phillips (1972) and Price & Hancock (1972).

The present work is a numerical evaluation of a theoretical model of a hydraulic fracture to provide a basis for the understanding and interpretation of the formation of natural hydraulic fractures during the deformation of rocks, and stems in particular from studies of syntectonic veins produced by hydraulic fracturing in deformed sedimentary rocks (e.g. Beach 1975, 1977).

Experimental studies of the fracture process and geometry in laboratory materials used as analogues to rocks are frequently limited to conditions of uniaxial stress and without the presence of a fluid in the crack (e.g. Brace & Bombalakis 1963, Hoek & Bieniawski 1965, Lajtai 1971). Similarly, theoretical studies of rock fracture often consider a crack under uniaxial stress only (Secor 1968,

Nomenclature—S1, S2 principal stresses applied at infinity; P fluid pressure within the crack; λ ratio P/S2; β orientation of crack long axis to applied stress S1; ζ_0 ellipse defining the periphery of the crack; C crack half length; σ_1, σ_2 principal stresses of the disturbed stress field generated around the flaw.

Cotterell 1972, Lajtai 1971, 1974). The extension of these models to shear fracturing has been considered for dry fractures by Hoek & Bieniawski (1965) and by Cotterell (1969, 1972). The work of Murell & Digby (1970a, b) therefore represents an important step forward in theoretical fracture studies, because these authors derive equations for stresses in three dimensions around the periphery of an ellipsoidal flaw under triaxial stress, with or without an internal fluid pressure, and also for conditions of crack closure. The recognition of many natural arrays of hydraulic shear fractures (Currie & Ferguson 1970, Phillips 1972, Shearman *et al.* 1972, Currie & Nwachukwu 1974, Moore 1975, Escher *et al.* 1976, Beach 1977, Price 1977) in deformed rocks makes it desirable to extend and evaluate models of fracture in this field.

The process of fracture growth in rocks is clearly complex. Firstly, it may involve slow crack extension under constant stress, called static fatigue (Martin 1972, Scholz 1972), and produced by stress corrosion at the crack tip (Wiederhorn 1967, Wiederhorn & Bolz 1970, Evans 1974, Evans & Johnson 1975, cf. Bieniawski 1967, fig. 1). Secondly, fracture growth may involve formation, interaction and coalescence of tensile and shear microfractures (Scholz 1968, Tchalenko 1968, Lajtai 1971, 1974) and thirdly, very rapid crack growth, generating shock waves (Price 1968, Gash 1971) and additionally, crack forking (Cotterell 1965, 1966, Bieniawski 1967) may occur. Many natural rock fractures are seen as extensive, single fracture surfaces, and whilst Lajtai (1977) discusses the origin of such features as tensile fractures, the problem of the origin of single shear fracture surfaces, in contrast to a zone of microfractured and damaged material traversed by a through-going shear fault (Lajtai 1971, Murrell 1977), is not clearly understood. Such fractures are commonly seen as joints (Price 1959, Lajtai 1977) in rocks, and also as the filled fractures of veins and dykes, etc. The work discussed in this paper is largely concerned with models that help understand the origin of single shear fracture surfaces through the mechanism of hydraulic fracturing.

Ideas on the fracturing of rocks and many other materials (cf. Liebowitz 1972) usually reduce to the concepts of stress concentrations at a crack tip (treated by Inglis 1913) and energy balance during crack growth (introduced by Griffith 1921). The model normally chosen for the crack is that of a narrow elliptical cavity in an isotropic elastic medium subjected to a uniform stress at infinity. One approach to the theory of fracture is to equate the (tensile) stress concentration at or near the crack tip to the theoretical strength of the material. A second approach assumes that the change in strain energy as a crack grows is at least equal to the energy associated with the formation of new crack surfaces (and related dissipative effects).

The extensive and detailed work of Murrell & Digby (1970a, b, 1972) has shown that the prediction of fracture initiation from a knowledge of the maximum tensile stress developed on the periphery of an ellipsoidal flaw in an elastic medium is the most valid approach. They show that the three-dimensional ellipsoidal flaw is not essentially different from the two-dimensional elliptical flaw, and that crack initiation from a flaw is independent of the magnitude of the applied intermediate principal stress, a factor built into many theories of rock fracture (see Murrell 1977). Further, Murrell & Digby (1972) show that the idea that a reduction in strain energy allows fracture initiation is a necessary but not a sufficient condition for crack propagation from a flaw, but that the condition that the local maximum tensile strength on the crack periphery equals the bond strength of the material is a sufficient condition for crack initiation. In this work, both stress and strain energy models are used.

THE MODEL

Use has been made of the stress function (that is, a function of X, Y that satisfies the conditions of static equilibrium and the biharmonic equation for elastic strain compatibility, and the second partial derivatives of which give the stress components σ_x, σ_y, τ_{xy} within the boundaries chosen: see Timoshenko & Goodier 1951) giving a numerical solution to the stresses and displacements around an elliptical crack under uniaxial stress, as given by Pollard (1973b), cf. Koide & Bhattacharji (1975). The model for a crack with internal fluid pressure under biaxial compression is then built up as follows, applicable to hydraulic fracturing in porous media where the law of effective stress applies throughout. The stresses around the ellipse are calculated separately for applied uniaxial effective stress S1–P and S2–P at orientations β and $\beta+90^\circ$ respectively, and summed to give the stresses around the crack under biaxial compression. The stresses around the same ellipse in the absence of applied stresses at infinity but containing an internal hydrostatic pressure (P) are then added to the previous result, and the desired model is then obtained. The detailed evaluation of the stress function for uniaxial stress is taken from Pollard (1973b). That for the internal hydrostatic stress is not given by Pollard, and equations derived by P. Gash (personal communication) are used (cf. Pollard & Johnson 1973). Thus the model presented here differs from that used by Pollard (1973a) because the application here is to hydraulic fracturing in rocks where the fluid phase permeates throughout the rock, rather than being confined entirely to the crack, as with the magmatic sheet intrusions discussed by Pollard.

Initially, a Cartesian framework is defined with the crack extending along the X-axis. The points at which stresses are required around the crack are defined in terms of X, Y. The coordinates are then transformed into elliptical co-ordinates ξ, η, because the stress function is evaluated in terms of them. The ellipse $\xi_0(=0.01$ throughout this paper) defines the crack boundary. In terms of Cartesian co-ordinates, crack half-lengths are allowed to vary from 1 to 10 along X. The stress equations are solved at each intersection of integer X, Y grid lines in fields from X, $Y = 30$, 30 to 80, 50. This ensures that the disturbed stress field around the crack has fallen to the regional

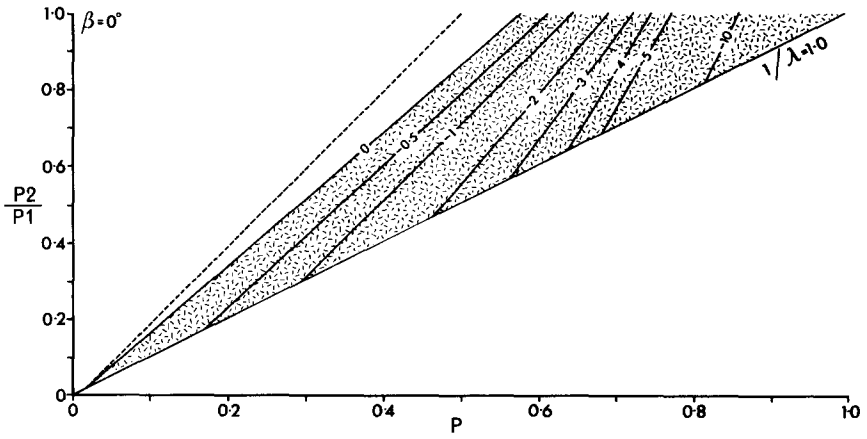

Fig. 1. Figures 1–4 show graphs of applied effective stress against crack internal pressure for $\beta = 0, 30, 60$ and 90° respectively. Values of the minimum stress off the crack are contoured, and the field where these stresses are tensile (negative) is shaded. To the right of the dashed line, this minimum stress is positioned symmetrically at the crack tip. Figure 1 is for $\beta = 0°$. Maximum applied effective stress in all figures = 1.0.

applied stresses by the time the edge of the field is reached (cf. Pollard 1973a). Programmes have been written in Fortran to carry out the lengthy calculations involved.

STRESS DISTRIBUTION AROUND HYDRAULIC FRACTURES

Using the criterion that fracture initiation occurs from points of maximum tensile stress generated by elliptical flaws, the stress distribution around elliptical hydraulic flaws is examined with particular reference to the generation of tensile stresses at crack tips and the prediction of fracture growth from such data.

The results are presented firstly in terms of the magnitude of the minimum stress off the crack tip. A number of workers (e.g. Cotterell 1965, Lajtai 1972) have suggested that while in theory the magnitude of the maximum tensile stress around a flaw rises with proximity to the crack tip, high stresses predicted by the theory near the tip are unrealistic and in practice would be dissipated by plastic deformation. Lajtai (1972) suggests that the stress generated a short (arbitrary) distance off the tip is a more reliable and realistic guide to the stress perturbation and condition of crack initiation from the flaw. In this work, with stresses calculated at integer values of X, Y and with the crack lying along $X = 10.5$ to $+10.5$, the closest position to the crack tip is the point $X = 11$, $Y = 0$ (cf. index in Fig. 5), this being an arbitrary decision to accord with the idea of Lajtai (1972). The position at which the minimum value of σ_2 (negative stress is tensile) generated around the flaw is found. For many conditions of applied effective stress the position of the minimum stress lies symmetrically off the crack, a situation found only when $\beta = 0°$ for cracks without an internal fluid pressure (Hoek & Bieniawski 1965, Lajtai 1971). The results are shown in Figs. 1–4 separately for the different crack orientations $\beta = 0$, 30, 60 and 90°. The graphs are plotted as the ratio of applied effective stresses against the value of the fluid pressure, and the magnitude of the minimum stress off the crack for these conditions is then contoured, the field where this minimum stress is tensile (−ve) being shaded in the figures. In addition, the dashed lines on the figures separate the fields of symmetrically developed minimum stress from the fields of asymmetrically developed minimum stress. If the tensile stress is of sufficient magnitude

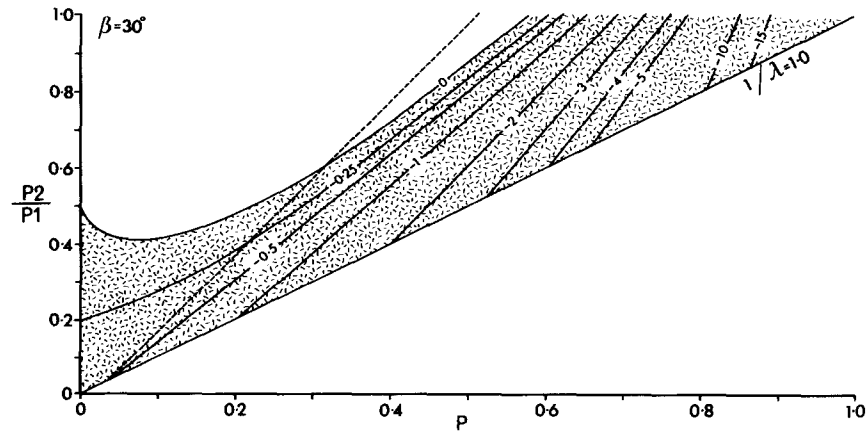

Fig. 2. $\beta = 30°$ (also see Fig. 1).

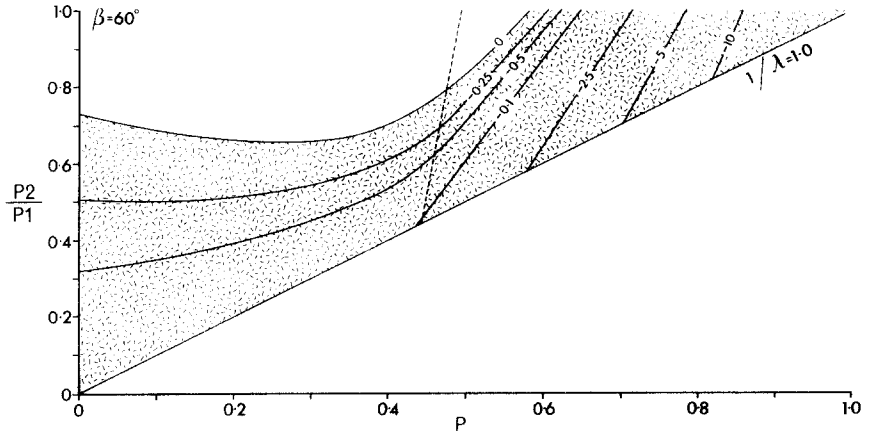

Fig. 3. $\beta = 60°$ (also see Fig. 1).

to cause failure, these lines represent the transition from symmetrical to asymmetrical failure of a crack of given orientation. This is not the same as the transition from tensile to shear failure discussed by Murrell & Digby (1970a) in terms of the relative magnitudes of the stresses applied at infinity.

Using the criterion that fracture propagation occurs from the point of maximum tensile stress, the data in Figs. 1–4 show that for many conditions of applied effective stress and orientation, both shear and tensile hydraulic fractures may initially propagate along their length. This is clearly important for a further understanding of the formation of single, straight shear fractures commonly observed in nature. Figure 1 is in agreement with results on dry fractures, while Fig. 2 presents a new concept to the extent that the maximum tensile stress is still positioned symmetrically at the crack tip for all conditions where λ is greater than 0.5 for the orientation of 30°. Figures 3 and 4 show that such symmetrically positioned maximum tensile stresses persist for high values of crack fluid pressure for orientations of 60 and 90°.

In Fig. 5 the data are replotted in terms of β vs λ, separately for the range of minimum applied effective stress. In these graphs the value of the minimum stress off the crack is contoured and the location of this stress recorded in terms of four separate positions around the crack as shown in the key to Fig. 5. This presentation emphasises the conditions for which a symmetrically located maximum tensile stress is developed. If it is assumed that a tensile stress at the flaw of magnitude $\sigma_2 = T = -1.0$ is needed to initiate fracture from the flaw, the magnitude of the crack fluid pressure needed to generate this tensile stress for given conditions of β and P2 can be shown as in the first graph of Fig. 6. Only the segements of the curves for each value of P2 for which the designated value of tensile stress is achieved are shown, the portions of these curves lying beneath the dashed line having this specified value of minimum stress located symmetrically at the crack tip (cf. Fig. 5). The other three graphs in Fig. 6 show the same relations as the first, but assume that a gradually decreasing value of minimum stress, $\sigma_2 = T = -0.75$, -0.5 and -0.25 respectively, represents the threshold for fracture initiation from the flaw.

From these curves it can be seen that at a given value of minimum applied effective stress P2, the magnitude of the fluid pressure within the crack needed to generate a given minimum stress off the crack varies considerably. These curves give an idea of the maximum values of fluid pressure that may exist in a series of variably oriented but unconnected flaws in a material at the threshold where

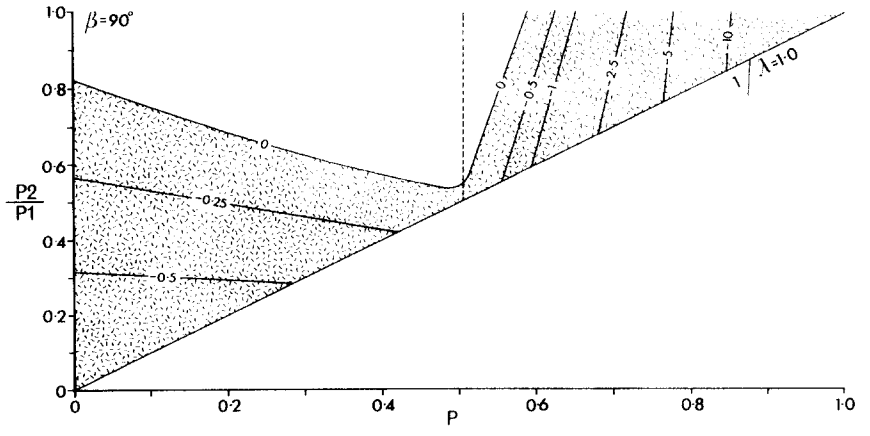

Fig. 4. $\beta = 90°$ (also see Fig. 1).

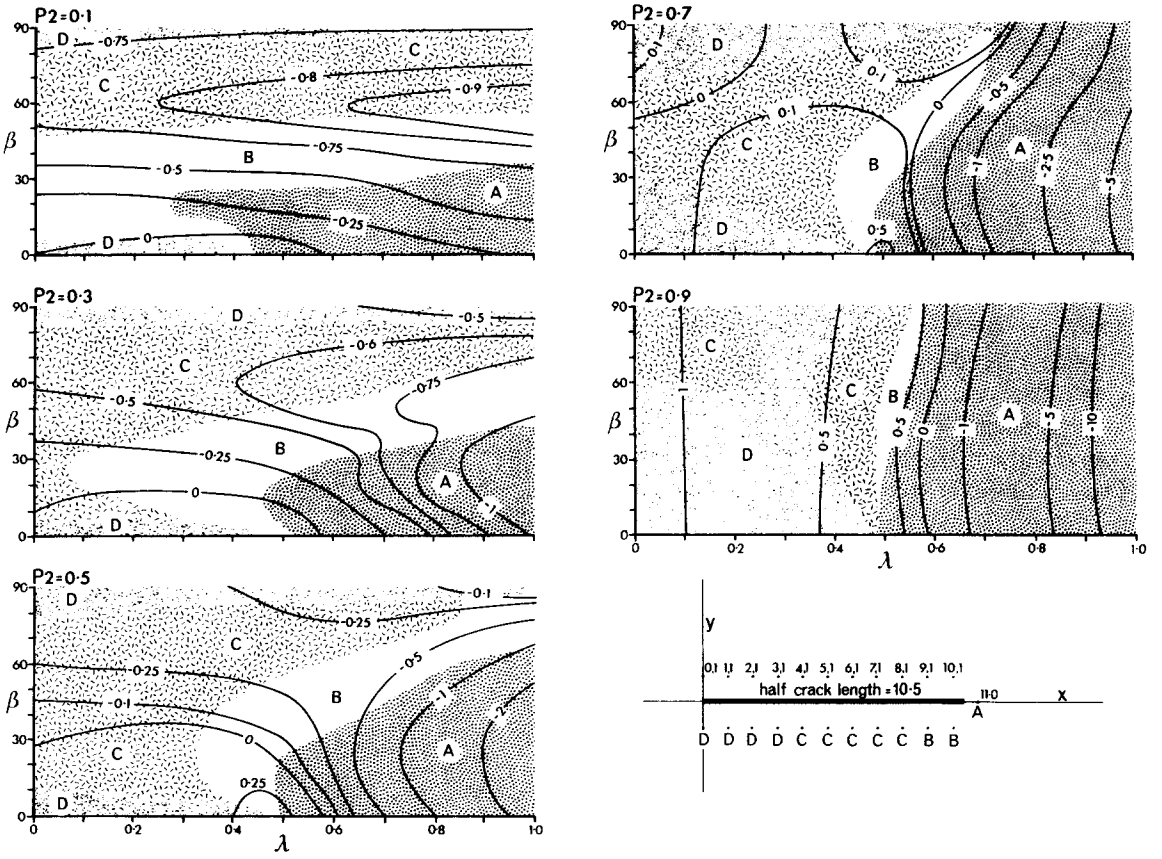

Fig. 5. Graph of β vs λ for five values of minimum applied effective stress P2 = 0.1, 0.3, 0.5, 0.7 and 0.9, with the magnitude of the minimum stress off the crack contoured, and its location indicated in terms of four positions A, B, C and D as defined in the key (bottom right).

one or more of these flaws is about to propagate. Thus, in the first graph of Fig. 6 cracks oriented at 90° are seen to be able to sustain higher fluid pressures than those at 30°, etc., and variations in fluid pressure throughout a material may exist. In contrast, if the fluid is not isolated in unconnected pores but has a more or less uniform pressure through a material, Fig. 6 will predict the orientation at which the tensile stress threshold for crack

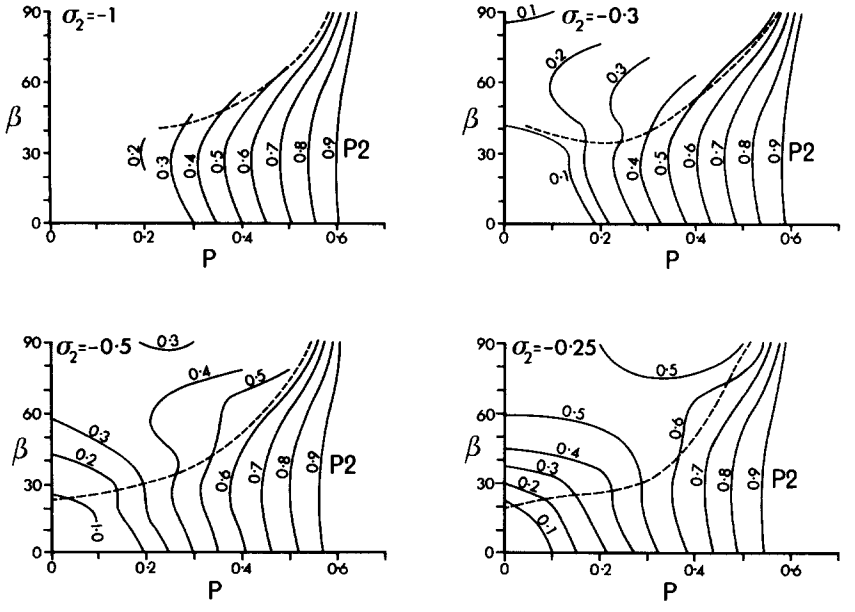

Fig. 6. Graphs of β vs P showing the conditions of minimum applied effective stress P2 needed to generate a minimum stress off the crack of $\sigma_2 = -1.0$, -0.75, -0.5 and -0.25 respectively. Below the dashed curve this minimum stress is developed symmetrically at the crack tip.

initiation will be reached for conditions of gradually rising fluid pressure and given applied effective stress P2. This problem is relevant to many geological situations where dehydration and a gradual rise in fluid pressure gives rise to fracturing of rocks, and it will be discussed further, later in the paper.

CALCULATION OF STRAIN ENERGY

Murrell & Digby (1972) show that the minimum stress criterion is a sufficient condition for prediction of fracture initiation, and that fracture initiation, involving a reduction in stored elastic strain energy, constitutes a necessary but not a sufficient condition for this process (cf. Perkins & Krech 1968). Elastic strain energy fields around hydraulic cracks and the second part of the Griffith criterion will be examined numerically.

Strain energy fields around cracks can be calculated directly from the stress models presented without any further assumptions. Stress components were calculated at each X, Y point on a regular grid around the elliptical flaw of length/width ratio of about 100/1 ($\xi_0 = 0{\cdot}01$). At each point the distortional and volumetric strain energy components were calculated using the standard relations, as given, for example, by Jaeger & Cook (1969, p. 116). These are then summed for all the X, Y points in the field examined to give the total distortional and volumetric strain energy around the crack. From these are subtracted the values of the strain energy over the field considered due to the application of the biaxial effective stresses at infinity in the absence of a crack. The result is the change in strain energy on introducing a crack of specified length and orientation into the area over which the calculations were carried out. This is referred to as the energy of formation of the crack. To be meaningful, the field of calculation must extend sufficiently far away from the crack that the magnitudes of the stresses σ_1, σ_2 have returned to the regional or applied stress magnitudes (cf. Pollard 1973). In this work, crack half lengths lying along $X = 0 \rightarrow 0.5$ to $0 \rightarrow 9.5$ in a field $X = 0 \rightarrow +80$, $Y = -25 \rightarrow +25$ are considered, and the stresses and strain energies calculated at every integer X, Y grid intersection, with the crack centre at $X, Y = 0$. The values of the elastic moduli used in the strain energy calculations are constant, and the strain energy values reported should be used as relative values only, recording increases or decreases in stored elastic strain energy during initial fracture formation and fracture growth.

The results of two different uses of the strain energy model are reported here. Firstly, consideration is given to the question of whether the introduction of a small crack into a previously unflawed elastic medium is accompanied by a reduction in stored strain energy, and hence whether such flaws are formed spontaneously and stably. Secondly, the problem of growth from small stable flaws is examined by calculating the change in stored strain energy as the crack half-length is allowed to increase under constant applied stresses, fluid pressure and orientation.

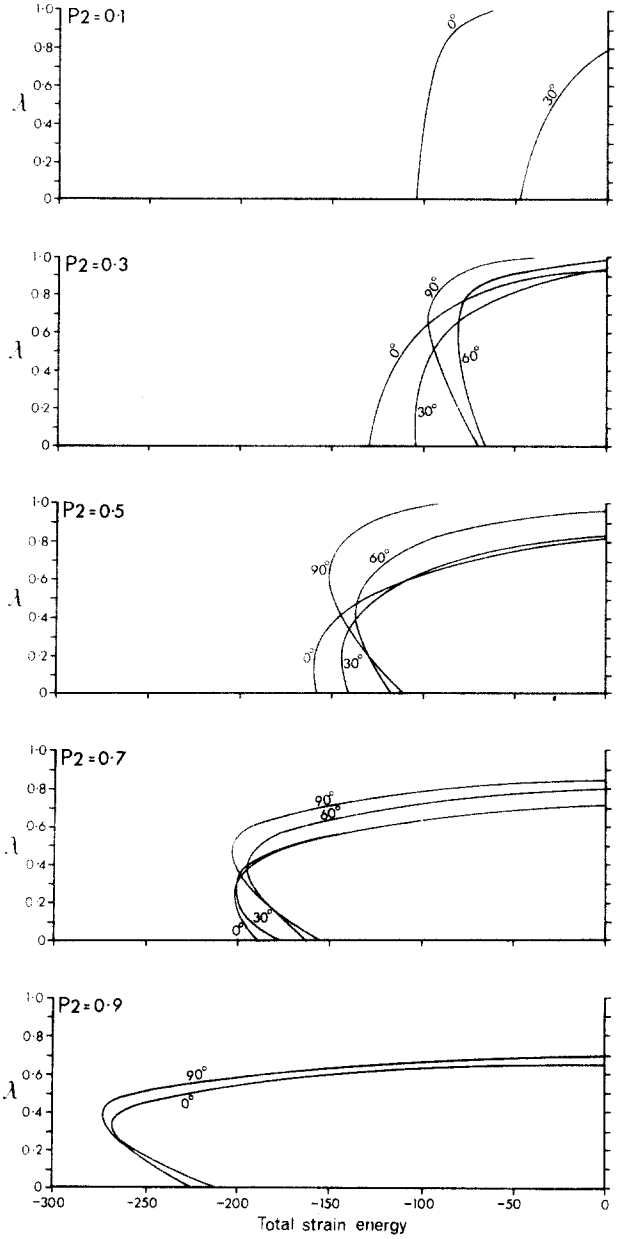

Fig. 7. Curves for each crack orientation on separate graphs for each value of minimum applied effective stress P2 showing the variation in strain energy of formation with the magnitude of λ of a short crack of constant half-length ($C = 1.5$).

RESULTS

Figure 7 shows the change in stored strain energy associated with the introduction (i.e. formation) of a small crack of constant half-length ($C = 1.5$). The graphs are plotted separately for each value of minimum applied effective stress P2 as λ vs change in strain energy, and on each graph a curve is shown for each orientation of the flaw 0, 30, 60 and 90°. Only those portions of the curves where a reduction in strain energy occurs are shown on these graphs. They therefore represent the range of conditions for which the spontaneous formation of a flaw is energetically possible.

Figure 7 also illustrates a further important point when natural hydraulic fracturing is being considered. Much

natural hydraulic fracturing occurs in response to dehydration and fluid release during progressive metamorphism of sedimentary sequences, and will therefore result from a gradual rise in crack fluid pressure causing fracture instability. Taking a small crack, such as that used in constructing Fig. 7, as a starting point, the effect of fluctuations (in particular increases) in crack fluid pressure, and hence λ, on the stability of the small crack may be assessed from the energy point of view.

Thus those portions of the curves in Fig. 1 with negative slopes indicate the conditions under which the total strain energy around the flaw decreases with a small increase in λ. For example, when P2 = 0.1, only the orientations $\beta = 0 \rightarrow 30°$ show a negative energy of formation, but there is an increase in strain energy with increase in λ. However, when P2 = 0.3, all orientations $\beta = 0 \rightarrow 90°$ show a negative energy of formation, and the orientations $60 \rightarrow 90°$ show a decrease in strain energy with increases in λ up to $\lambda = 0.5$–0.6.

Such cracks are therefore able to accommodate an increase in λ, because this is accompanied by a decrease in stored strain energy. This is an equivalent expression of dilatancy hardening, recorded experimentally (cf. Edmond & Patterson 1972, Ismail & Murrell 1976) as a rising stress difference with increased strain at constant fluid pressure, for the more natural conditions of rising fluid pressure under constant applied effective stress that may exist in many rocks during metamorphism and burial (cf. Norris & Henley 1976). Once the positively sloping portions of the curves in Fig. 1 are entered beyond the strain energy minima shown, then a small increase in fluid pressure in the crack results in an increase in stored strain energy, and the increased fluid pressure cannot therefore be accommodated. The turning points of these graphs thus mark the points at which the flaw may become unstable and fracture initiation may occur in response to the increased fluid pressure, provided that the necessary tensile stress for rupture exists at the crack tip. Reference to the results presented earlier will show if this condition is satisfied.

The second part of the problem referred to above must now be examined, that is, having reached the point of fracture initiation and instability, which orientations of the small crack are able to undergo spontaneous growth by increasing their length. The criterion used is that the total strain energy must decrease for growth to be spontaneous. The results reported here are for cracks increasing in half-length from $C = 1.5$ to $C = 9.5$, the change in stored strain energy being calculated for each increase in half-length of 1.0. The crack shape was maintained at $\xi_0 = 0.01$ and the results are shown as graphs of strain energy vs crack half-length, for specified conditions of λ, P2, and β. The fluctuations and changes in fluid pressure that might accompany very rapid crack extension have not been examined here, and the conditions modelled are those of rather slower growth that is dependent on the maintenance of a constant fluid pressure as the driving mechanism for hydraulic fracture. In practice the volume of fluid in the crack and the crack shape itself may change; the conditions of hydraulic fracture growth imply that fluid is able to migrate into the crack to maintain the fluid pressure in order that crack extension may proceed. This point will be developed further.

Table 1. Values of λ above which the minimum stress at the crack tip is located symmetrically to the crack

P2	$\beta=0$	10	20	30	40	50	60	70	80	90
0.1	0.44	0.41	0.29	0.77	—	—	—	—	—	—
0.3	0.52	0.47	0.46	0.58	0.87	—	—	—	—	—
0.5	0.50	0.49	0.48	0.56	0.67	0.75	0.85	—	—	—
0.7	0.49	0.49	0.50	0.54	0.58	0.63	0.66	0.71	0.71	0.71
0.9	0.50	0.50	0.50	0.51	0.53	0.55	0.56	0.57	0.58	0.58

Clearly, the model employed here can only be evaluated numerically for those situations where the crack grows in a straight line along its length, and the growth of curved fractures, etc. cannot be modelled, though some qualitative statements concerning their origin can be made (see later). Thus only those cracks that have a symmetrically oriented minimum stress at their tips will be examined quantitatively. The relevant conditions, corresponding to

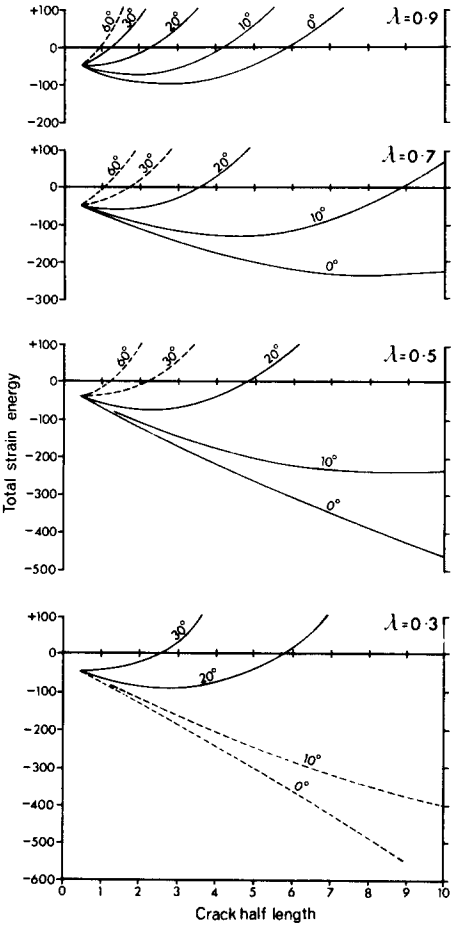

Fig. 8. Figures 8–12 show the variation in strain energy with increase in crack half-length for P2 = 0.1, 0.3, 0.5, 0.7 and 0.9 respectively. Each figure shows separate graphs for different values of λ, and each graph has curves for different crack orientations. The solid curves are those orientations, etc. for which the minimum stress is located symmetrically at the crack tip. The dashed curves are for comparison and qualitative discussion only as for these the minimum stress is positioned asymmetrically at the crack tip. See Fig. 2—P2 = 0.1.

field A in Fig. 5, for which this occurs are given in Table 1. Finally, the growth model described and evaluated is a quasi-static one and cannot be applied to those cracks where dynamic effects become important.

The results of the numerical analysis are shown in Figs. 8–12 where the change in strain energy with increasing crack length is plotted for each orientation, and each figure is for a different value of minimum applied effective stress P2, as indicated. The solid curves are for those orientations which have a minimum stress developed symmetrically at their tips (cf. Table 1). The dashed lines are for asymmetrically positioned minimum stress and are shown to indicate the conditions where the transition from symmetrical to asymmetrical minimum stress might occur.

The set of results presented in Figs. 8–12 show a number of features. Most of the relevant (i.e. solid line) curves are concave upwards in these graphs i.e. $d^2W/dc^2 > 0$, where W = stored strain energy. Clearly dW/dc is negative, falls to zero and then becomes positive and begins to increase in magnitude (a few curves are close to straight lines, e.g. Fig. 12, and the positions where $dW/dc = 0$ have not been defined within the space of the graph shown). During the gradual increase in crack length, growth occurs spontaneously when $dW/dc < 0$. From the minimum point onwards, energy would have to be supplied from outside the system to allow further growth. The crack length at which $dW/dc = 0$ provides an estimate of the relative length of spontaneous crack growth. For example, it is easy to distinguish between conditions and orientations where spontaneous growth is quickly arrested and where crack growth occurs freely for some length. This summarises the principal way in which these results help to understand the growth of hydraulic fractures.

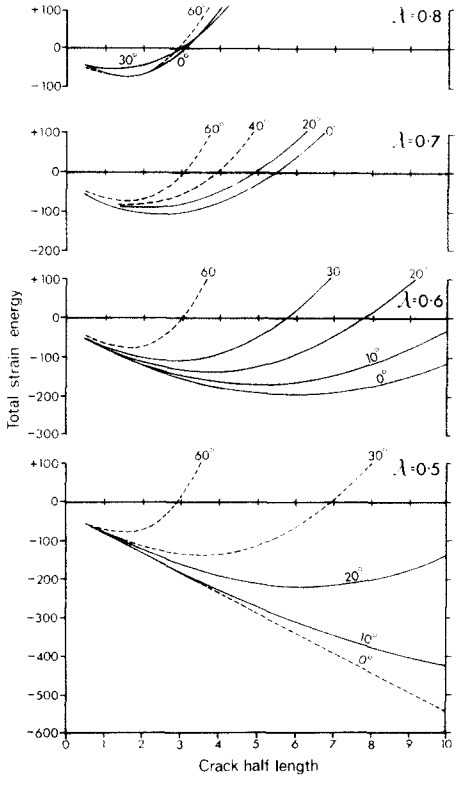

Fig. 9. P2 = 0.3 (also see Fig. 8).

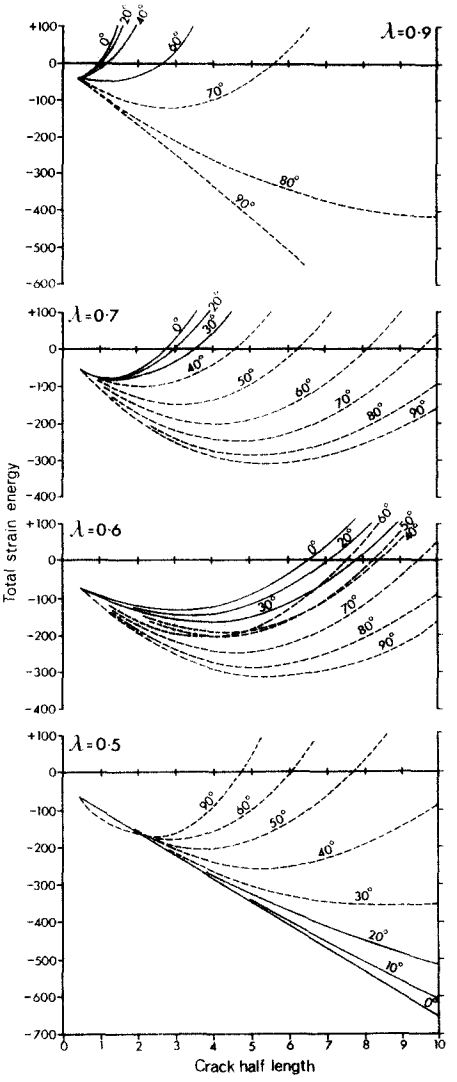

Fig. 10. P2 = 0.5 (also see Fig. 8).

SYNTECTONIC VEINS AS HYDRAULIC FRACTURES

The results presented so far were obtained in order to further the understanding of the formation of hydraulic fractures under symmetrical and oblique biaxial loading conditions, with particular reference to the formation of syntectonic veins, frequently observed to have formed in abundance during the deformation of sedimentary sequences at low metamorphic grades. The build up of high pore fluid pressures, a necessary prerequisite for hydraulic fracturing, in buried sediments has been discussed by Rubey & Hubbert (1959). Clay mineral reactions involving dehydration will maintain high pore pressures during subsequent low grade metamorphism (Magara 1975b, Hower *et al.* 1976). In addition, if sedimentary rocks are buried along a geotherm greater than about 12°/km, water will expand and contribute to sustaining these high

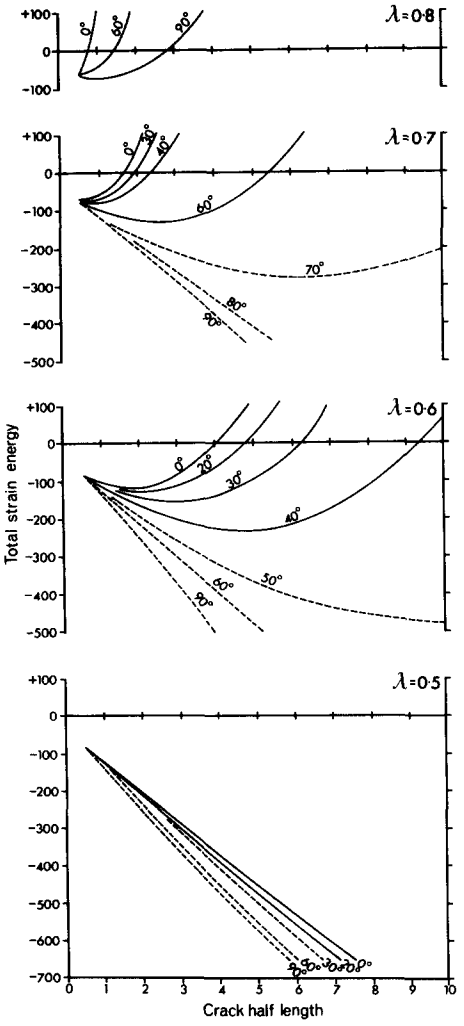

Fig. 11. P2 = 0.7 (also see Fig. 8).

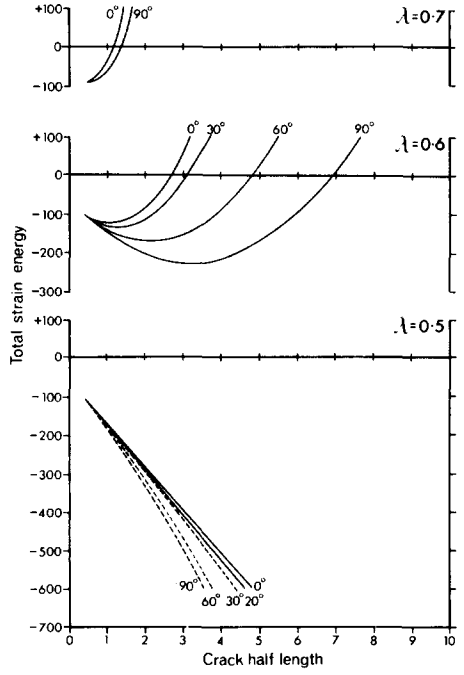

Fig. 12. P2 = 0.9 (also see Fig. 8).

pore pressures (Magara 1975a, Norris & Henley 1976). Thus the formation of hydraulic fractures should be a natural consequence of burial and metamorphism of sedimentary sequences in most geological environments.

During the burial of sediments the effective stresses will be approximately hydrostatic and equal to lithostatic pressure, that is in terms of the model employed here, P1 ~ P2 ~ 1.0. During deformation of these sedimentary rocks the effective stress difference will gradually increase, that is, in the present model P1 is held constant and P2 decreases. If dewatering of the sediments does not keep pace with burial and metamorphism, the value of λ will gradually rise (cf. Rubey & Hubbert 1959). Thus the main cause of the onset of hydraulic fracture instability in such rocks will be a rise in λ to the point where the minimum stress at a crack tip exceeds the tensile strength of the material, in contrast to the rising stress difference employed to induce fracturing in laboratory experiments (cf. Ismail & Murrell 1976, Phillips 1972). It is considered that in the natural conditions under discussion, a rise in fluid pressure is more important than a change in stress difference in causing hydraulic fracture, and thus the diagrams presented earlier have been drawn mostly with this mode of interpretation in mind. Within this framework, the numerical results obtained will now be applied to the interpretation of syntectonic hydraulic fractures.

Many syntectonic hydraulic fractures in deformed sedimentary rocks are preserved by infillings of quartz, carbonate, etc. as veins. That such natural fractures originated as hydraulic fractures is most easily demonstrated when the fractures are shear fractures and when they originated during a compressive deformation. Convincing examples have been documented by Escher *et al.* (1976) for magmatic dykes, and by Beach (1977) for syntectonic veins. The compressive deformation in sedimentary rocks during the formation of syntectonic veins under low grade metamorphic conditions is usually accomplished by pressure solution (Rutter 1976, Kerrich *et al.* 1977) and the silica etc. in solution in the sedimentary rock migrates to the slightly lower fluid pressure in the fracture and crystallises to form a vein, creating a natural outlet for much of the material dissolved during deformation (Beach 1974, 1975, Kerrich *et al.* 1978).

A number of easily recognisable geometric forms are common in such syntectonic veins: (a) single, straight shear and tensile veins of considerable length, usually with length/width > 500; (b) short, straight or slightly curved shear and tensile veins, usually with length/width < 100; (c) single veins with a zig-zag trace; (d) curved branches originating perpendicularly to a vein near its termination; (e) vein terminations that may be singly tapering, or forked into many thin veins; (f) offset veins; and (g) en échelon veins.

APPLICATION OF THE NUMERICAL RESULTS

Symmetric minimum stress at crack tip

The analysis has shown that a tensile stress field is

Table 2. Critical crack orientation 20–30°. To create the minimum stress σ_2 specified, at a given value of P2, the values of λ entered are required

	P2 =	0.2	0.3	0.4	0.5	0.6	0.7	0.8	0.9
σ_2 =	−1.00	0.95	0.85	0.78	0.73	0.70	0.68	0.67	0.67
	−0.75		0.75	0.71	0.68	0.67	0.66	0.65	0.64
	−0.50				0.63	0.63	0.63	0.63	0.62
	−0.25					0.58	0.60	0.60	0.60

developed at the crack tip for many values of λ less than 1.0 under a variety of applied stress conditions and for a variety of orientations (Fig. 5). Thus if the failure criterion is satisfied hydraulic shear fractures may grow when $\lambda < 1.0$. The tensile stress is developed symmetrically at the crack tip for many orientations and for a wide range of λ values, and it is inferred that such cracks will grow in a straight line along the prolongation of the original crack. From Fig. 6 it is possible to assess the orientation of the critical crack, that is, the crack that will grow first for given applied stress and with a gradually increasing value of λ. For $\sigma_2 = T = -1.0$ it is seen that the critical orientation is $\beta = 20$–$30°$. If fracture occurs when a smaller magnitude of tensile stress is developed at the crack tip, say $\sigma_2 = T = -0.25$, the critical orientation is still $\beta = 20$–$30°$ for P2 = 0.6–0.9, but is variable for P2 < 0.6 (see Fig. 6). The fields of symmetrically developed minimum stress (from Fig. 5) are shown on the graphs in Fig. 6 to determine whether or not the critical cracks have a symmetric minimum stress. Thus, straight fractures of orientation $\beta = 20$–$30°$ may be expected to form when P2 = 0.2–0.9 if the stress threshold for fracture is $\sigma_2 = -1.00$, when P2 = 0.3–0.9 if $\sigma_2 = -0.75$, when P2 = 0.5–0.9 if $\sigma_2 = -0.50$ and when P2 = 0.6–0.9 if $\sigma_2 = -0.25$ (see Fig. 6). The values of λ giving rise to these conditions are given in Table 2.

The critical conditions in Table 2 may now be examined in conjunction with Figs. 8–12 to determine whether these cracks will grow on the basis that growth requires a decrease in strain energy, and that the minimum points in the curves of Figs. 8–12 therefore represent the limit of spontaneous growth of the crack under the conditions specified. Following this interpretation, it is found that the conditions in Table 2 give rise to spontaneous growth producing crack half-lengths as summarised in Table 3.

Beyond this limit of spontaneous crack growth under constant applied effective stress and fluid pressure conditions, an interpretation of the mechanism of continued crack growth is considered; the mechanism is a qualitative adaptation of the model to natural conditions likely to occur during hydraulic fracture propagation, that is, a drop in fluid pressure occurs during fracture growth, resulting from the increased volume of the crack. The slope of the strain energy vs crack length curves will change as follows (Figs. 8–12).

(i) At P2 = 0.9 and 0.7, a decrease in λ from 0.6 to 0.5 changes the slope of the curves drastically, and these curves lose their minima, allowing effectively infinite crack extension to occur spontaneously; for P2 = 0.9 only, the curves are concave downwards (Fig. 12) and the energy release rate increases with crack length.

(ii) At P2 = 0.5, a decrease of λ towards 0.5 increases the length of spontaneous crack growth, though the curve for the critical crack $\beta = 20°$ is seen (Fig. 10) to be concave upwards and the energy release rate will decrease to zero during growth.

(iii) At P2 = 0.3, a decrease of λ to 0.6 and then to 0.5 increases the length of crack growth by only a small amount (see Fig. 9); the curves are all concave upwards and shorter fractures will be formed under these conditions compared with (i) and (ii) above.

Table 3. Half-lengths of spontaneous growth for critical crack conditions given in Table 2

	P2 =	0.2	0.3	0.4	0.5	0.6	0.7	0.8	0.9
σ_2 =	−1.00		1.0		1.5		1.0		0.5
	−0.75		1.5		2.5		1.5		0.7
	−0.50				3.5		2.5		1.0
	−0.25						3.0		1.5

Asymmetric minimum stress at crack tip

Whilst the stress function analysis used permits evaluation only of straight crack growth, some qualitative consideration can be given to situations where the minimum stress is positioned asymmetrically at the crack tip.

An existing fracture with an asymmetric minimum stress will undergo further crack growth by propagating a branch fracture (Brace & Bombalakis 1963, Hoek & Bieniawski 1965, Adams & Sines 1978), which leaves the main crack at right angles to its edge at the point of maximum tensile stress and curves towards the orientation of the maximum applied stress as it grows. Branch fractures are common in syntectonic veins (cf. Beach 1977) and may be a product of second stage growth from master veins. An example is illustrated in Fig. 13.

However, Figs. 8–12 indicate some further conditions under which branch fracturing may occur. When the energy release rate decreases during crack growth (curves concave upwards), fractures will terminate as single tapering structures if the minimum stress remains symmetrically positioned at the crack tip (Fig. 14). If such a fracture develops an asymmetric minimum stress during growth, it may terminate by curving and tapering, and may also produce one or two well defined branch fractures (Fig. 15). These structures form the most unequivocable evidence that the main fracture originated as a shear fracture. Such branch fractures will have an infilling that is continuous in structure etc. with the main vein, in contrast to secondary branch fracturing where the texture and/or mineralogy of the infilling may be different from that of the main vein.

Bieniawski (1967) has described the formation of terminal crack forking as a means of dissipating excess strain energy and kinetic energy released during very rapid crack growth for tensile fractures, that is as a

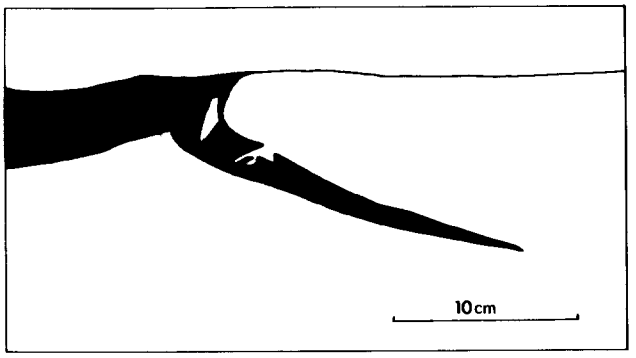

Fig. 13. Typical geometry of branch fracture; Lias slates, La Grave, Hautes Alpes.

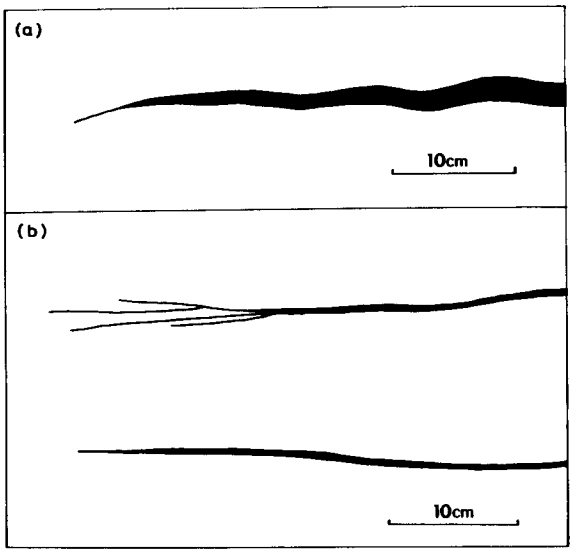

Fig. 14. Single tapering vein terminations: (a) is from the Lias limestone shale, La Grave, Hautes Alpes—the slight sinuosity is where the vein crosses limestone and shale beds, and (b) is from Devonian sandstone, Healey Pass, Co. Kerry—the adjacent vein, also shown, has a forked termination (cf. Figs. 16 and 17).

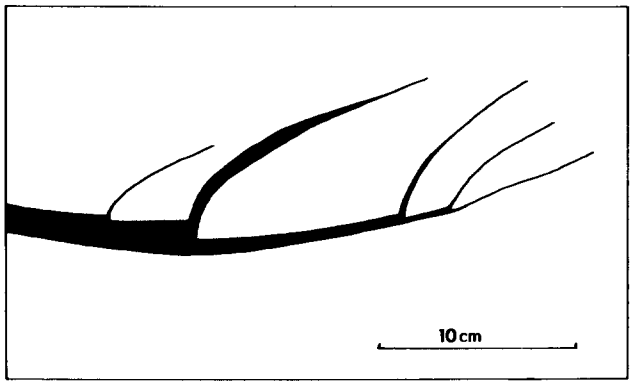

Fig. 15. Vein terminating by slight curvature and development of successive branch fractures; Carboniferous flysch, Millook Haven, N. Cornwall.

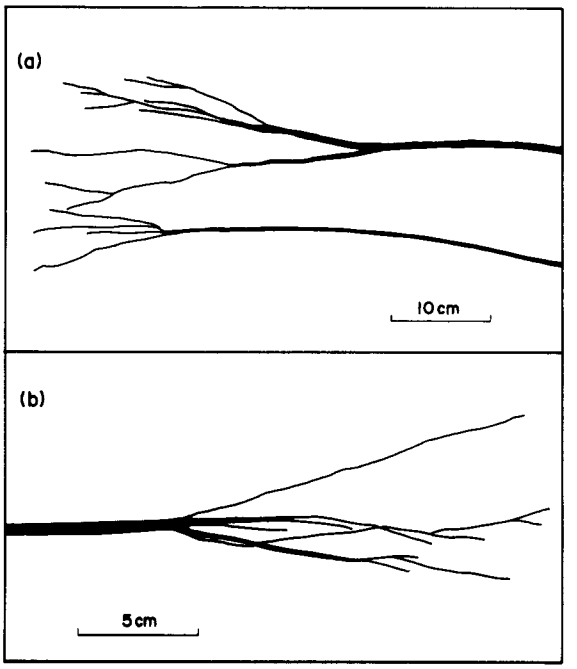

Fig. 16. Examples of symmetrically forked terminations to veins; in (a) two adjacent veins are illustrated, in (b) the geometry at the termination of a vein is shown in more detail; both examples from Devonian sandstone, Healey Pass, Co. Kerry.

product of dynamic crack growth. That terminal forking of both shear and tensile hydraulic fractures is predicted for certain conditions by the quasi-static growth model evaluated here is seen from examination of Figs. 8–12. Those curves that are concave downwards on these figures are interpreted as indicating that an increase in the rate of decrease of stored strain energy accompanies crack growth. Such an increase in energy release rate results, as with the dynamic problem studied by Bieniawski (1967), in terminal forking of the fracture to dissipate the excess energy by the large increase in the formation of fracture surfaces. A distinction can be made between symmetric and asymmetric forking.

If the minimum stress remains symmetrically positioned at the crack tip, then this forking should be symmetrically developed with respect to the main fracture (Fig. 16). Under other conditions, again with the energy release rate increasing during growth, the minimum stress may become asymmetrically positioned at the crack tip (e.g. Fig. 12, when P2 = 0.9 and λ decreases from 0.6 to 0.5 during growth, orientations of $\beta = 30$–$90°$ develop an asymmetric minimum stress; another example is seen in Fig. 11 when $\beta = 40°$ and λ decreases to 0.5). Such cracks should terminate by forking asymmetrically with respect to the main fracture (Fig. 17). Branch fractures (Figs. 13 and 15), as propagations from main fractures, commonly terminate as simple tapered structures, but may also show symmetric or asymmetric forking more characteristic of main fractures growing under conditions of increasing energy release rate, and examples of these features are shown in Fig. 18.

In addition to the critical orientations deduced from Fig. 6 and discussed above, Figs. 8–12 indicate that

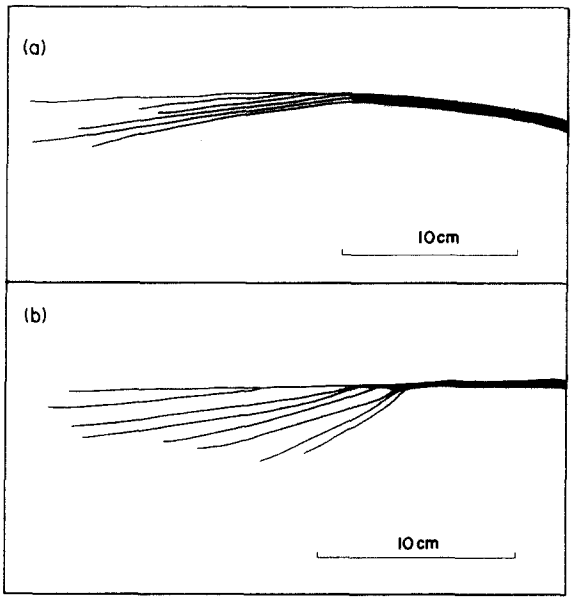

Fig. 17. Two examples of veins terminating by asymmetric forking, both from the Eocene flysch near Lautaret and Valfroide, Hautes Alpes. In (a) the main vein is slightly curved, in (b) it is straight.

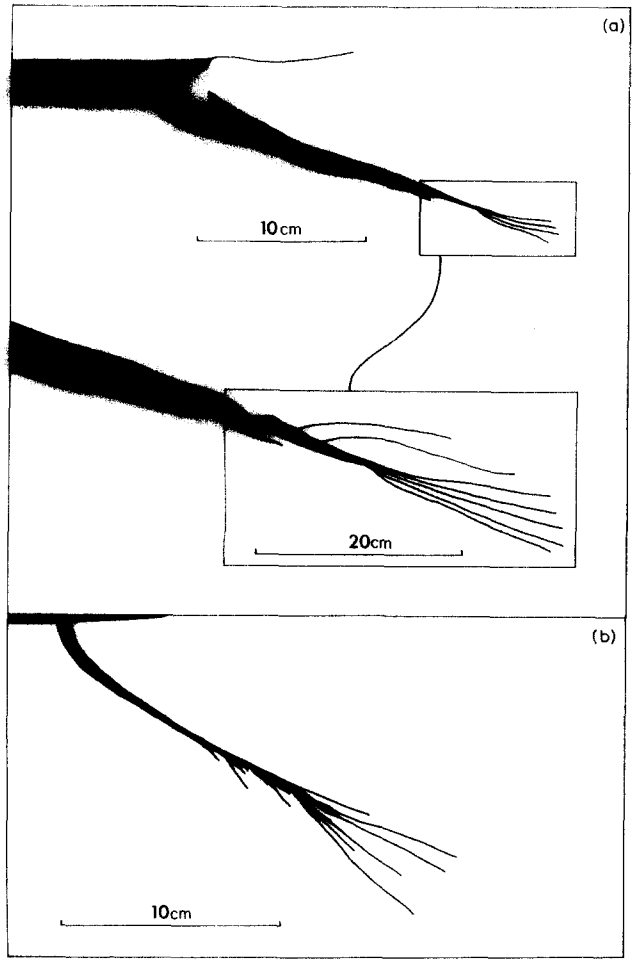

Fig. 18. Terminal forking of branch fractures (cf. Fig. 15). (a) Shows a more or less symmetrical forking of a branch fracture from the Lias shales, near Rivet, Hautes Alpes—the inset shows an enlargement of the termination. (b) Shows distinctly asymmetric forking of a branch fracture from the Eocene flysch above Lautaret, Hautes Alpes.

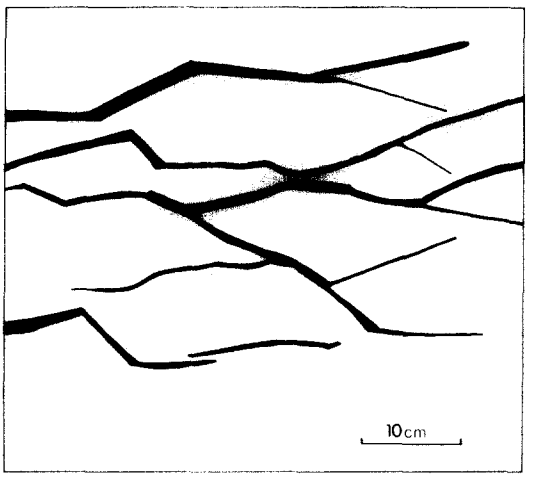

Fig. 19. Irregular zig-zag geometry of veins from Carboniferous flysch, Millook Haven, N. Cornwall.

spontaneous growth of other orientations may also occur, as follows.

(i) When P2 = 0.9 (low stress difference) growth of all orientations may occur, and as λ decreases during growth, extensive propagation results; when $\beta < 30°$ symmetric forking is expected to form and when $\beta > 30°$ asymmetric forking should form. When P2 = 0.7 similar results are expected.

(ii) When P2 = 0.1 (high stress difference), symmetric growth of orientations $\beta < 30°$ and branching of orientations $\beta > 30°$ should occur. As λ decreases during growth, extensive propagation of the $\beta = 0°$ orientation will occur. Growth of orientations β = 10–20° will be limited as the curves (Fig. 8) pass through a minimum, and shorter, straight fractures will form. When P2 = 0.3, similar results are expected.

(iii) Under the intermediate condition when P2 = 0.5, branching from orientations $\beta > 40°$ will occur. As λ decreases, an increasing length of symmetric growth for β = 0–30° will occur. At first, the 30° orientation grows most, but as λ decreases, the 0° orientation undergoes extensive growth, possibly terminating in symmetric forking.

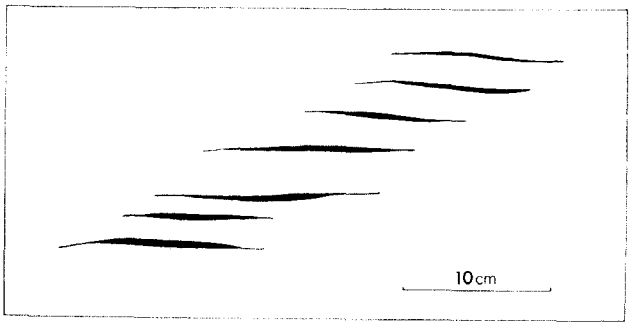

Fig. 20. En échelon arrangement of simply tapering veins from Cretaceous sandstone, Galibier, Hautes Alpes.

DISCUSSION AND CONCLUSIONS

The model used in this work is in essence a simple one and it is as well at this stage to repeat its limitations. The analysis is two-dimensional and assumes that the crack is elliptical in shape and that the surrounding material is isotropic and elastic. The model does not deal with either curving cracks or with cracks that are so close that they interact. In spite of the simplicity of the model it is felt that the theoretical results do help in understanding the growth of hydraulic fractures in porous rocks under effective applied stress.

Tapering, curving, branching and forking are important fracture geometries and their origin has been interpreted in terms of the quasi-static changes in stored strain energy during hydraulic fracture extension. Also, the commonly observed occurrence of long straight hydraulic shear fractures in deformed sedimentary rocks is explained by the maintenance of a symmetrically positioned minimum stress at the fracture tip, a feature not found in dry shear fractures.

Continued spontaneous crack growth has been interpreted to result from a gradual drop in the fluid pressure in the crack as a natural consequence of increasing crack growth. If however the value of λ remains constant, or does not decrease sufficiently to allow extensive spontaneous crack growth, then the fracture will be arrested when the rate of change in stored strain energy becomes positive. The fracture may become infilled by the precipitation of quartz, etc., the stress conditions at which spontaneous growth originally occurred may return, and a further short extension to the fracture may take place. A number of possible fracture geometries may arise under these conditions, none of which can be adequately explored using the results of the present model. Possibly the fracture will propagate along its length again, or it may grow by forming a branch fracture, as already explained and illustrated. However, continued periods of crack growth may give rise to formation of a zig-zag geometry, or under some conditions the first fracture may be sufficiently stabilised that renewed fracture growth occurs by successive formation of new fracture symmetrically related to the first and giving rise to en échelon patterns. These last two geometries are illustrated in Figs. 19 and 20.

Cotterell (1965, 1966) has discussed the stability and direction of fracture extension for cracks in tension, and notes that a crack may grow in a straight line along its length, diverge widely from this, or diverge and then return alternately giving a regular zig-zag pattern. The stability of the crack growth is related to the distribution of the lines of equal shear stress around the fracture tip, and the model employed here could be extended to evaluate this feature for hydraulic fractures as an aid to understanding some of the more irregular fracture geometries such as that illustrated in Fig. 19.

Finally, whilst only hydraulic shear fractures can develop asymmetric terminal forking, a curved trace or branch fractures—related to the asymmetrically positioned minimum stress—their absence does not necessarily indicate that a fracture originated as a tensile crack, because under many of the conditions evaluated in this work, hydraulic shear fractures, like tensile fractures, have a symmetrically positioned minimum stress and both may terminate as single tapered or as symmetrically forked structures. Extensive growth of hydraulic shear fractures is most likely to occur under conditions of relatively low differential stress, and short shear fractures will form when the stress difference is relatively higher. Extensive growth of hydraulic tensile fractures may occur throughout the range of applied effective stresses used in this model.

It is hoped that the interpretations presented here of natural fractures in terms of a numerical model will lead both to a more detailed study of the geometry of veins and other hydraulic fractures and to further development of the theoretical work.

Acknowledgements—I would like to thank L. Wilson (Lancaster) and D. Pollard (U.S.G.S.) for their help with some of the analytical problems encountered in the early stages of this work. P. Gash freely gave of his advice and his evaluation of the hydrostatic stress function used here, for which I am very grateful. Extensive computer time on the CDC7600 at UMRCC was provided by Liverpool University. I thank Joe Lynch for his careful drawing of all the graphs and Helen Moorcraft for reading an early version of this work. Some of the fieldwork which has provided the stimulus for this work was supported by NERC grant GR3/3472.

REFERENCES

Adams, M. & Sines, G. 1978. Crack extension from flaws in a brittle material subjected to compression. *Tectonophysics* **49**, 97–118.

Beach, A. 1974. A geochemical investigation of pressure solution and the formation of veins in a deformed greywacke. *Contr. Mineral. Petrol.* **46**, 61–68.

Beach, A. 1975. The geometry of en échelon vein arrays. *Tectonophysics* **28**, 245–263.

Beach, A. 1977. Vein arrays, hydraulic fractures and pressure solution structures in a deformed flysch sequence, S.W. England. *Tectonophysics* **40**, 201–225.

Bieniawski, Z. T. 1967. Mechanism of brittle fracture of rock, III experimental studies. *Int. J. Rock Mech. & Mining Sci.* **4**, 407–423.

Brace, W. F. & Bombalakis, E. G. 1963. A note on brittle crack growth in compression. *J. geophys. Res.* **68**, 3709–3713.

Cotterell, B. 1965. On brittle fracture paths. *Int. J. fracture Mech.* **1**, 96–103.

Cotterell, B. 1966. Notes on the paths and stability of cracks. *Int. J. fracture Mech.* **2**, 526–533.

Cotterell, B. 1969. The paradox between the theories for tensile and compressive fracture. *Int. J. fracture Mech.* **5**, 251–252.

Cotterell, B. 1972. Brittle fracture in compression. *Int. J. fracture Mech.* **8**, 195–208.

Currie, J. B. & Nwachukwu, S. O. 1974. Evidence of incipient fracture porosity in reservoir rock at depth. *Bull. Can. Petrol. Geol.* **22**, 42–58.

Currie, K. L. & Ferguson, J. 1970. The mechanism of intrusion of lamprophyre dykes indicated by offsetting of dykes. *Tectonophysics* **9**, 525–535.

Edmond, J. M. & Paterson, M. S. 1972. Volume changes during the deformation of rocks at high pressures. *Int. J. Rock Mech. & Mining Sci.* **9**, 161–182.

Escher, A., Jack, S. & Watterson, J. 1976. Tectonics of the north Atlantic dyke swarm. *Phil. Trans. R. Soc.* **A280**, 529–540.

Evans, A. G. 1974. Slow crack growth in brittle materials under dynamic loading conditions. *Int. J. Fract.* **10**, 251–259.

Evans, A. G. & Johnson, H. 1975. The fracture stress and its dependence on slow crack growth. *J. Mater. Sci.* **10**, 214–222.

Fyfe, W. S. 1976. Chemical aspects of rock deformation. *Phil. Trans. R. Soc.* **A283**, 221–228.

Gash, P. J. 1971. A study of surface features relating to brittle and semi-brittle fracture. *Tectonophysics* **12**, 349–391.

Griffith, A. A. 1921. The phenomena of rupture and flow in solids. *Phil. Trans. R. Soc.* **A221**, 163–198.

Haimson, B. C. & Fairhurst, C. 1967. Initiation and extension of hydraulic fractures in rocks. *AIME Petrol. Trans.* **240,** 310–318.
Hoek, E. & Bieniawski, Z. T. 1965. Brittle fracture propagation in rock under compression. *Int. J. fracture Mech.* **1,** 137–155.
Holland, J. G. & Lambert, R. St. J. 1969. Structural regimes and metamorphic facies. *Tectonophysics* **7,** 197–217.
Howard, G. C. & Fast, C. R. 1970. Hydraulic fracturing. *Soc. Petrol. Eng. AIME* monograph **2,** 1–23.
Hower, J., Eslinger, E. V., Hower, M. E. & Perry, E. A. 1976. Mechanism of burial of argillaceous sediment: I. mineralogical and chemical evidence. *Bull geol. Soc. Am.* **87,** 725–737.
Hubbert, M. K. & Willis, G. W. 1957. Mechanics of hydraulic fracturing. *AIME Petrol. Trans.* **210,** 153–168.
Inglis, C. E. 1913. Stresses in a plate due to the presence of cracks and sharp corners. *Trans. R. Instn nav. Archit.* **55,** 219–230.
Ismail, I. A. H. & Murrell, S. A. F. 1976. Dilatancy and the strength of rocks containing pore water under undrained conditions. *Geophys. J. R. astr. Soc.* **44,** 107–134.
Jaeger, J. C. & Cook, N. G. W. 1969. *Fundamentals of Rock Mechanics.* Methuen, London.
Kerrich, R., Beckinsale, R. D. & Durham, J. J. 1977. The transition between deformation regimes dominated by intercrystalline diffusion and intracrystalline creep evaluated by oxygen isotope thermometry. *Tectonophysics* **38,** 241–257.
Kerrich, R., Beckinsale, R. D. & Shackleton, N. J. 1978. The physical and hydrothermal regime of tectonic vein systems: evidence from stable isotope and fluid inclusion studies. *Neues Jb. Miner. Abh.* **131,** 225–239.
Koide, H. & Bhattacharji, S. 1975. Formation of fractures around magmatic intrusions and their role in ore localisation. *Econ. Geol.* **70,** 781–799.
Lajtai, E. Z. 1971. A theoretical and experimental evaluation of the Griffith theory of brittle fracture. *Tectonophysics* **11,** 129–156.
Lajtai, E. Z. 1972. Effect of tensile stress gradient on brittle fracture initiation. *Int. J. Rock Mech. & Mining Sci.* **9,** 569–578.
Lajtai, E. Z. 1974. Brittle fracture in compression. *Int. J. Fract.* **10,** 525–536.
Lajtai, E. Z. 1977. A mechanistic view of some aspects of jointing in rocks. *Tectonophysics* **38,** 327–338.
Liebowitz, H. 1972. *Fracture—An Advanced Treatise—Vol. 7, Fracture of Non-metals and Composites.* Academic Press, New York.
Lutton, R. J. 1971. Tensile fracture mechanics from fracture surface morphology. In : *Dynamic Rock Mechanics, Proc. 12th Symp. Rock Mechanics* (edited by Clark, G. B.), 561–571.
Magara, K. 1975a. Importance of aquathermal pressuring effect in Gulf Coast. *Bull. Am. Ass. Petrol. Geol.* **59,** 2037–2045.
Magara, K. 1975b. Re-evaluation of montmorillonite dehydration as cause of abnormal pressure and hydrocarbon migration. *Bull. Am. Ass. Petrol. Geol.* **59,** 292–302.
Magara, K. 1976. Water expulsion from clastic sediments during compaction—direction and volumes. *Bull. Am. Ass. Petrol. Geol.* **60,** 543–553.
Martin, R. J. 1972. Time dependent crack growth in quartz and its application to the creep of rocks. *J. geophys. Res.* **77,** 1406–1419.
Moore, J. McM. 1975. A mechanical interpretation of the vein and dyke systems of the S.W. England orefield, *Miner. Deposita* **10,** 374–388.
Murrell, S. A. F. 1977. Natural faulting and the mechanics of brittle shear failure. *J. geol. Soc. Lond.* **133,** 175–189.
Murrell, S. A. F. & Digby, P. J. 1970a. The theory of brittle fracture initiation under triaxial stress conditions—I. *Geophys. J. R. astr. Soc.* **19,** 309–334.
Murrell, S. A. F. & Digby, P. J. 1970b. The theory of brittle fracture initiation under triaxial stress conditions—II. *Geophys. J. R. astr. Soc.* **19,** 499–512.
Murrell, S. A. F. & Digby, P. J. 1972. The thermodynamics of brittle fracture initiation under triaxial stress conditions. *Int. J. Fracture Mech.* **8,** 167–173.
Norris, R. J. & Henley, R. W. 1976. Dewatering of a metamorphic pile. *Geology* **4,** 333–336.
Perkins, T. K. & Krech, W. W. 1968. The energy balance concept of hydraulic fracturing. *AIME Petrol. Trans.* **243,** 1–12.
Phillips, W. J. 1972. Hydraulic fracturing and mineralisation. *J. geol. Soc. Lond.* **128,** 337–359.
Pollard, D. D. 1973a. Derivation and evaluation of a mechanical model for sheet intrusions. *Tectonophysics* **19,** 233–269.
Pollard, D. D. 1973b. Equations for stress and displacement fields around pressurised elliptical holes in elastic solids. *J. Int. Assoc. math. Geol.* **5,** 11–25.
Pollard, D. D. 1979. On the mechanical interaction between a fluid-filled fracture and the earth's surface. *Tectonophysics* **53,** 27–57.
Pollard, D. D. & Johnson, A. M. 1973. Mechanics of growth of some laccolithic intrusions in the Henry Mountains, Utah—II. *Tectonophysics* **18,** 311–354.
Price, N. J. 1959. Mechanics of jointing in rocks. *Geol. Mag.* **96,** 149–167.
Price, N. J. 1968. A dynamic mechanism for the development of second order faults and related structures. *Geol. Surv. Pap. Can.* **68–52,** 49–78.
Price, N. J. 1975. Fluids in the crust of the earth. *Sci. Prog., Lond.* **62,** 59–87.
Price, N. J. 1977. Aspects of gravity tectonics and the development of listric faults. *J. geol. Soc. Lond.* **133,** 311–327.
Price, N. J. & Hancock, P. L. 1972. Development of fracture cleavage and kindred structures. *Proc. 24th Int. Geol. Congr.* **Sect. 3,** 584–592.
Rubey, W. W. & Hubbert, M. K. 1959. Role of fluid pressure in mechanics of overthrust faulting, II. *Bull. geol. Soc. Am.* **70,** 167–206.
Rutter, E. H. 1976. The kinetics of rock deformation by pressure solution. *Phil. Trans. R. Soc.* **A283,** 203–220.
Scholz, C. H. 1968. Experimental study of the fracturing process in brittle rock. *J. geophys. Res.* **73,** 1447–1454.
Scholz, C. H. 1972. Static fatigue of quartz. *J. geophys. Res.* **77,** 2104–2114.
Secor, D. T. 1968. Mechanics of natural extension fracturing at depth in the earth's crust. *Geol. Surv. Pap. Can.* **68–52,** 3–48.
Shearman, D. J., Mossop, G., Dunsmore, H. & Martin, M. 1972. Origin of gypsum veins by hydraulic fracture. *Trans. Inst. Min. Metall.* **81,** B149–B155.
Tchalenko, J. S. 1968. The evolution of kink bands and the development of compression textures in sheared clays. *Tectonophysics* **6,** 159–174.
Timoshenko, S. & Goodier, H. N. 1951. *Theory of Elasticity.* McGraw-Hill, New York.
Wiederhorn, S. M. 1967. Influence of water vapour on crack propagation in soda-lime glass. *J. Am. Ceram. Soc.* **50,** 407–414.
Wiederhorn, S. M. 1968. Moisture assisted crack growth in ceramics. *Int. J. Fracture Mech* **4,** 171–177.
Wiederhorn, S. M. & Bolz, L. H. 1970. Stress corrosion and static fatigue of glass. *J. Am. Ceram. Soc.* **53,** 543–548.